Simulation of Spatters Sticking Phenomenon in Laser Powder Bed Fusion Process Using the Smoothed Particle Hydrodynamics Method

Lingbin Meng[1], Tao Sun[2], Jing Zhang[1*]

[1]Department of Mechanical and Energy Engineering, Indiana University-Purdue University Indianapolis, Indianapolis, IN 46202, USA

[2] Department of Materials Science & Engineering, University of Virginia, Charlottesville, VA 22904, USA

*Corresponding author: jz29@iupui.edu

Abstract

In this work, a smoothed particle hydrodynamics (SPH) based model is developed to simulate the spattering phenomenon in the laser powder bed fusion (L-PBF) process. Spattering is a physical phenomenon in the L-PBF process observed from experiments and is found to be one of the major causes of structural defects in printed products. To alleviate it, researchers have made unremitting efforts in experiments to investigate the spattering phenomenon.

This work develops an SPH model to simulate the spatter sticking phenomenon observed from the experiment using the high-speed synchrotron X-ray to monitor the L-PBF process. The high-speed synchrotron X-ray full-field imaging experiments are performed on beamline 32-ID-B at the Advanced Photon Source (APS), Argonne National Laboratory.

For the SPH model, for simplification, two particles from the experiment are selected to be simulated, and their trajectories from the simulation are then compared with the experimental results for model validation. Different particles represent the substrate, metal vapor, and metal powders. The parameters related to the initial magnitude and direction of the velocity of the particles are defined such that the configuration can resemble the typical scenario. The procedure of the model is summarized as follows. First, an experiment using the high-speed synchrotron X-ray full-field imaging is conducted to acquire the *in situ* images during the L-PBF process. Then, a scenario is selected from a sequential X-ray image for the SPH model. In this study, a particle is ejected and melted by the metal vapor, impacts with another particle solidifies and sticks to the other particle to form a rigid body. As a result, the trajectories of the two particles match well with the experimental observation. The evolution of velocity and temperature of the particle is extracted

This is the author's manuscript of the article published in final edited form as:
Meng, L., Sun, T., Dube, T., Sagar, S., Yang, X., Zhang, J., & Zhang, J. (2022, January 25). Simulation of Spatters Sticking Phenomenon in Laser Powder Bed Fusion Process Using the Smoothed Particle Hydrodynamics Method. ASME 2021 International Mechanical Engineering Congress and Exposition. https://doi.org/10.1115/IMECE2021-66761

from the simulation for analysis. The results show that the SPH model can resemble the trajectories of the particles and simulate the sticking phenomenon observed in the experiment. The simulation result matches well with the experimental result. The L-PBF process involves physical phenomena including heat transfer, phase change, and particle motion, which is difficult to be simulated in one computational model like computational fluid mechanics. The phase change is done by the particle type change capability in the model when certain conditions, such as solidus and liquidus, are matched. In spite of the assumption of an infinite rate of phase change, the SPH simulation package with an adjustable rate of phase change may be included. The SPH model can be a useful alternative to computational models of simulating the spattering phenomenon of L-PBF.

Keywords: additive manufacturing; smoothed particle hydrodynamics; spatter.

1. Introduction

Laser powder bed fusion (L-PBF) is a popular additive manufacturing (AM) technique for metallic materials, due to the capability of producing parts with improved density, resolution, and surface finish that require less post-processing compared to other AM processes such as binder jetting [1]. In a typical L-PBF process, a recoating blade first pushes a layer of fresh powder from the powder reservoir to the top of the previously built surface or the substrate. Then, a laser beam passes through a system of lenses and is reflected by a mirror that controls the laser beam spot moving along the designed path to selectively melt the metal powder. This process is repeated in a layer-by-layer manner.

Spattering is a physical phenomenon in the L-PBF process observed from experiments [2, 3] and is found to be one of the major causes of the structural defects in printed products [4, 5].. To alleviate it, forerunners have made unremitting efforts in experiments to investigate the spattering phenomenon. Zhao *et al*. [6] applied high-speed synchrotron X-ray to monitor the L-PBF process of Ti-6Al-4V *in situ*, and found that some spatters tend to merge together and form larger particles. Andani *et al*. [7] used SEM images to quantify the spatters sizes and their distribution during PBF process with multi-laser technology. Through the comparison between multi-laser and single laser scanning, they found that a higher number of working laser beams induces greater recoil pressure above the melting pools and thus more spatters are ejected from the molten pool. In addition, the spatter particles size was found to be much larger than the raw powders. Large spatters tend to create an inclusion or remain as a non-melted region into the printed part, and thus degrade its quality [7]. Guo *et al*. [8] used in-situ high-speed high-energy x-ray imaging to detailedly study the spattering mechanism and quantification as a function of time, environment pressure, and location in the L-PBF process. Under stationary laser impulse, as time goes by, the vaporization occurs after melting and generates intensive vapor jet which ejects the metal powders, and then argon gas flow forms and forces the particles surrounding the molten pool to move toward the molten pool. If the pressure of the surrounding argon gas is decreased, the intensity of the argon gas flow will also decrease, and thus powders are ejected with a large divergence angle as the vapor can expand freely. Regarding the effect of location, the experiment was conducted under moving laser beam at normal pressure. They found that particles behind the laser beam tend to move towards laser beam entrained by argon gas flow, particles around the laser beam tend to be ejected by the evaporation recoil pressure, and particles ahead of the laser beam tend to incline

towards the laser beam. Yin *et al*. [9] applied a laser confocal microscope to characterize the morphological features of Inconel 718 sample. The correlation between the laser power and the ejection angle was revealed by their study. Overall, the spattering mechanisms and its effect are well exposed by experiments.

Although the spattering mechanism is well exposed from experimental studies, simulation and modelling of the spattering phenomenon is still a challenge due to its multi-phase nature and complexity in physics. Pioneers have made efforts to simulate the L-PBF process using numerous computational models. These models range from nanoscopic model such as molecular dynamics (MD), and mesoscopic models such as computational fluid dynamics (CFD).

MD is a numerical method for studying the atomic motion and has been used to investigate the sintering behavior for nanoparticles [10-13]. For L-PBF, to achieve simulation using MD, metal particles are assumed to be scaled down to nanoscale. Yi Zhang *et al*. [14] applied different constant uniform temperature field to represent different laser power in their MD simulation of the sintering process of 41 well stacked nickel particles, and concluded that higher laser power will lead to higher resultant tensile strength. Yue Zhang *et al*. [15] applied non-translational kinetic energy to a moving laser spot using the "fix heat" method in LAMMPS to represent the laser energy in their MD simulation of $Cu_{50}Zr_{50}$ metallic glass in a simulated powder bed of 5*5 particles with a fix power density of 15.4 J/mm^2. The multi-layer sintering process was successfully simulated by their model. Despite of these efforts by forerunners, spattering phenomenon was not simulated by their MD models. Even under the scaling assumption, the scope of spattering phenomenon is still beyond the simulation capability of MD, due to its physical complexity.

CFD is a class of numerical methods aiming at solving problems involve fluid flows. As the L-PBF process involves molten pool dynamics, CFD models are frequently applied to simulate the sintering process in L-PBF. Khairallah *et al*. [16] developed a numerical simulation software tool, ALE3D, based on LBM and the arbitrary Lagrangian-Eulerian (ALE) techniques, and applied it to simulate the spattering phenomenon in L-PBF process [17-19]. Though liquid-phase spatters driven by the recoil pressure can be observed from their simulation results, solid particles are stationary and cannot be ejected in CFD models. In addition, the recoil pressure in all the simulations mentioned above is simulated by adding a boundary condition that reflects its effect, instead of simulating the vapor expansion. In this regard, Bidare *et al*. [20] simulated the argon gas flow induced by the metal vapor using a 2D finite element analysis (FEA) model, but powder

bed and molten pool dynamics were not included in their model, as it's not a CFD based model. Overall, though CFD models are suitable to simulate the molten pool dynamics, the fact that the solid metal powders can only be stationary in CFD model limits its application in simulating the spattering behavior in L-PBF process.

This work proposes a new feasibility of simulating the spattering phenomenon in the L-PBF process. A smoothed particle hydrodynamics (SPH) model is developed in this work to simulate the spattering phenomenon. The simulation includes the interaction between the metal vapor and the spatters, the melting and solidification of the metal powders and the sticking phenomenon observed in the experiment. The model is validated by a similar scenario in the experiment.

The structure of the rest of this article is organized as follows. Section 2 elaborates the SPH model and the experiment done by the Argonne National Laboratory. Section 3 focuses on a case study with similar configuration in the experiment. The simulation result is compared with the experimental result for validation. Section 4 summarizes the work and provides the future work suggestions.

2. Methodology

This work develops a SPH model to simulate the spatter sticking phenomenon observed from the experiment. For simplification, two particles from the experiment are selected to be simulated, and their trajectories from the simulation are then compared with the experimental results for model validation. In this section, the theory of the SPH model is briefly introduced in Section 2.1. Then, the experiment setting is described in Section 2.2.

2.1. Smoothed particle hydrodynamics model

SPH is a method to solve problems in Lagrangian continuum mechanics. It was developed by Gingold and Monaghan [21] and Lucy [22] in 1977, initially for astrophysical problems. Then, it was extended to solid mechanics by Libersky and Petschek [23, 24].

The governing equation of SPH fluid is the Euler equations of mass conservation and momentum balance:

$$\frac{d\rho}{dt} = -\rho\nabla \cdot \mathbf{v}; \tag{1}$$

$$\frac{d\mathbf{v}}{dt} = -\frac{1}{\rho}\nabla \cdot P; \tag{2}$$

$$\frac{de}{dt} = -\frac{1}{\rho}P:\nabla\mathbf{v} - \frac{1}{\rho}\nabla\cdot Q, \tag{3}$$

where ρ is the density, t is the time, $\mathbf{v}$ is the velocity vector, P is the pressure tensor, e is the energy per unit mass, and the heat-flux vector $Q = \kappa\nabla T$, with thermal conductivity κ and temperature gradient ∇T. SPH interpolates the set of field variables by means of kernel interpolation [25]. For any variable $f(r)$, a local average at each coordinate $\mathbf{r_i}$ is calculated according to [25]

$$f(\mathbf{r_i}) = \sum_j m_j \frac{f_j}{\rho_j} W(\mathbf{r_i} - \mathbf{r_j}). \tag{4}$$

Here, m_j is the mass of particle j. f_j is the value of the field $f(r)$ at position $\mathbf{r_j}$. ρ_j is the value of the mass density at $\mathbf{r_j}$. $W(\mathbf{r_i} - \mathbf{r_j})$, denoted by W_{ij}, is the kernel function of compact support and decays to zero within a range h comparable to a few typical inter-particle spacings. Since m_j, f_j, ρ_j are particle properties and are not affected by the gradient operator ∇, the only term that is affected by ∇ is W_{ij}.

The governing equation of SPH solid is the total Lagrangian formulation given by [26]:

$$\rho J = \rho_0; \tag{5}$$

$$\ddot{\mathbf{u}} = \frac{1}{\rho_0}\nabla_0 P^T; \tag{6}$$

$$\dot{e} = \frac{1}{\rho_0}\dot{\boldsymbol{F}}:\boldsymbol{P}. \tag{7}$$

Here, $\boldsymbol{P}$ is the first Piola-Kirchhoff stress tensor. The subscript 0 and the absence of the subscript indicate that a quantity is evaluated in the reference configuration and the current configuration, respectively. J is the determinant of the deformation gradient $\boldsymbol{F}$, given by [26]

$$F = \frac{d\mathbf{x}}{d\mathbf{X}} = \frac{d\mathbf{u}}{d\mathbf{X}} + I, \tag{8}$$

where $\mathbf{x}$ and $\mathbf{X}$ are the current coordinates and the reference coordinates, respectively, $\mathbf{u} = \mathbf{x} - \mathbf{X}$ is the displacement, and I is the diagonal unit matrix. Same as the SPH fluid, SPH solid also uses Eq. (4) to evaluate variables in terms of the reference coordinates. For more detailed introduction to the SPH model, the reader is referred to the excellent book by Liu [27] and the guides by Ganzenmüller [25, 26].

This work utilizes the USER-SPH and USER-SMD packages [25, 26] in the Large-scale Atomic/Molecular Massively Parallel Simulator (LAMMPS) [28]. A missing capability in a typical SPH simulation is the phase change. In this work, a batch file in shell language is used to change the particle type to represent the melting and solidification. The melting is assumed to

finish once the liquidus is reached, and the solidification is assumed to finish once the solidus is reached. In other words, the rate of melting and solidification is assumed to be infinity. The latent heat is added to the particle for solidification and deducted from the particle for melting. The particle motion is simulated by the USER-SMD package and the heat transfer is simulated by the USER-SPH package.

2.2. Experimental setting

This work applies the high-speed synchrotron X-ray to monitor the L-PBF process. The high-speed synchrotron X-ray full-field imaging experiments are performed on beamline 32-ID-B at the Advanced Photon Source (APS), Argonne National Laboratory [29]. The laser system consists of an ytterbium fiber laser source (IPG YLR-500-AC, IPG Photonics, Oxford, Massachusetts, USA) integrated with a laser scanner (Intelli*SCAN*$_{de}$ 30, SCANLAB GmbH, Puchheim, Germany). The reader is referred to Ref. [29] for detailed information of the experimental apparatus. The Inconel 718 powders fabricated by the Praxair Inc. is used as the material. The recording rate is 50000 Hz.

A sample high-speed X-ray image acquired from the experiment is shown in Figure 1. A lot of ejected powders can be observed (Figure 1(b)). Among these ejected powder, some are melted and merged together to form large spatter (Figure 1(a)), and some stick with other powders (Figure 1(d)). This work focuses on simulating the sticking phenomenon observed from the experiment, in order to demonstrate its capability of simulating the phase change and heat transfer in the L-PBF process. Particle A and B are selected from this image for simulation, as they will stick with each other after several frames.

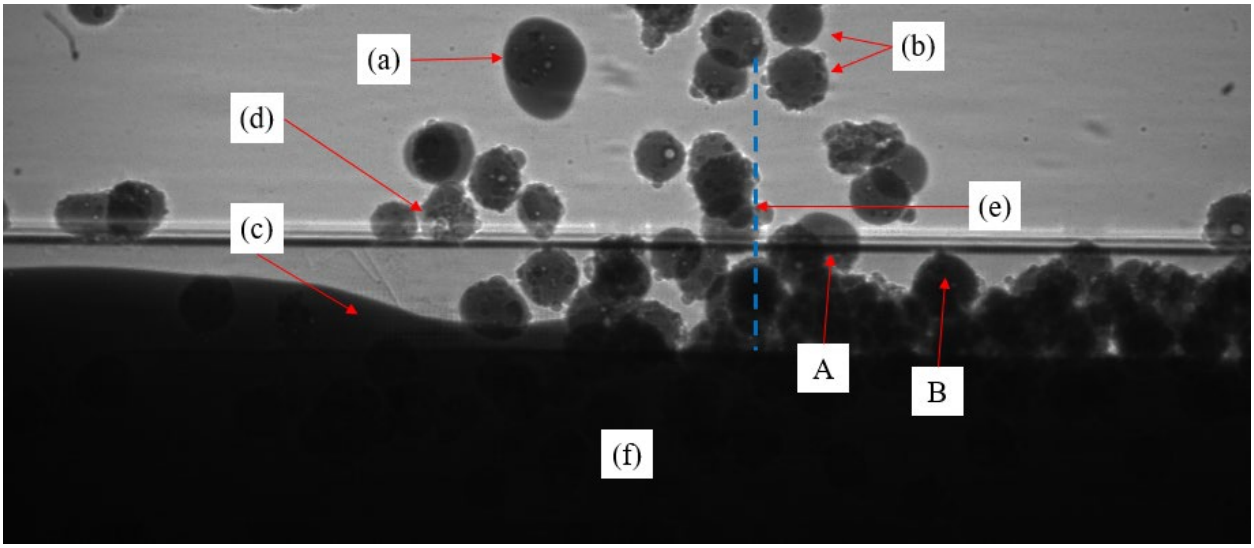

Figure 1. A sample high-speed X-ray image. (a) large spatter or molten metal ejected from the melt pool, (b) ejected powder, (c) molten pool, (d) stuck powders, (e) current laser scanning position, and (f) substrate. A and B represent to two particles selected from the experiment for simulation.

3. Results and discussion

3.1. Initial configuration

This work focuses on a 2-D case for simplification. The initial configuration is shown in Figure 2. The Open Visualization Tool (OVITO) [30] is used for visualization. Here, the yellow, red, and blue particles represent the substrate, metal vapor and metal powders. The parameters related to the initial magnitude and direction of the velocity of particle A are defined such that the configuration can resemble the typical scenario shown in Figure 1. These parameters including: powder diameter $d_p = 80$ μm, angle between vapor moving direction and horizontal line $\theta = 45°$, vapor initial speed $v_i = 500$ m/s, initial center to center distance between particle A and B $d_i = 240$ μm, initial temperature of vapor $T_g = 3000$ K, initial temperature of powders $T_A = 1300$ K, $T_B = 300$ K, vapor density $\rho_g = 0.02$ g/cm^3, and gravity $F_g = 9.81$ N/kg. Since the parameters related to the velocity of particle A has been used as an input in the simulation, only the interaction between particle A and B and their trajectories will be used for model validation.

The material parameters of Inconel 718 used in this work are listed as follows [31]: density $\rho = 8.19$ g/cm^3, Young's modulus $E = 204.9$ GPa, Poisson's ratio $\nu = 0.3$, thermal diffusivity $\alpha = 5.0$ mm^2/s, thermal conductivity $k = 11.4$ W/m · K, liquidus $T_l = 1609$ K, solidus $T_s = 1533$ K. The air is not modeled in this simulation, as the diffusion of gas is difficult to simulate in a typical SPH model. Therefore, the effect of air resistance and air cooling is ignored in this work.

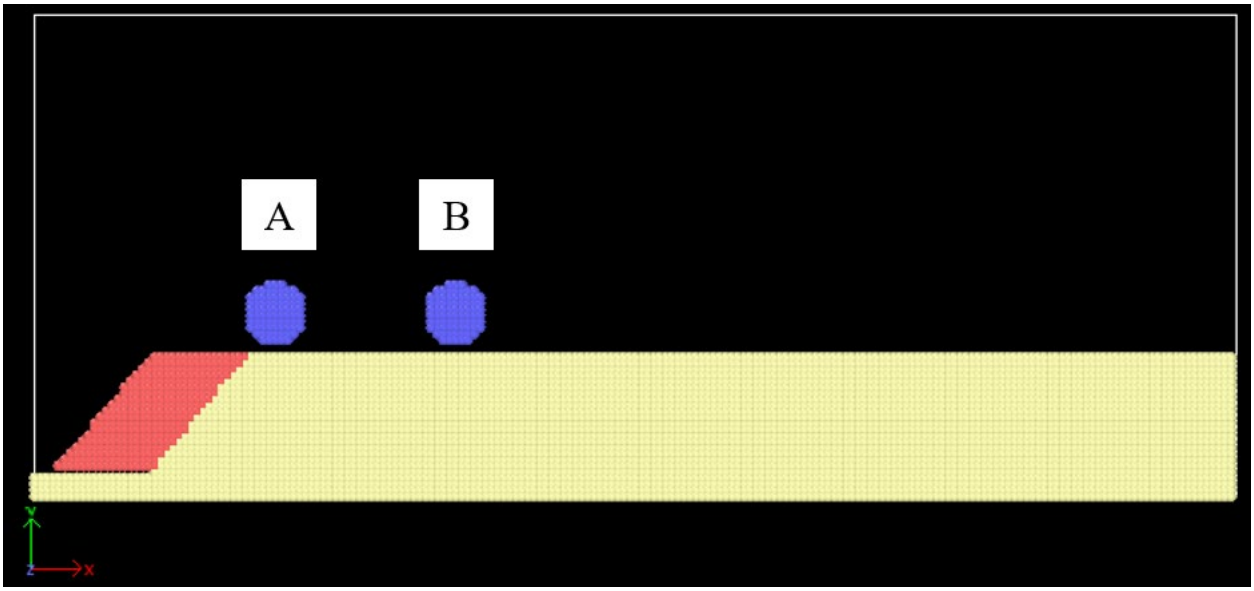

Figure 2. Initial configuration of the SPH model

3.2. Particle trajectories

The trajectories of particle A and B of the scenario in Section 3.2 are displayed in Figure 3. The time at Figure 3(a) is set to be $t_0 = 0$ ms. At 0 ms, particle A is interacting with the metal vapor, acquiring both kinetic energy and internal energy from the vapor. At 0.08 ms, particle A is melted, and keeps moving towards particle B. At 0.14 ms, particle A gets in contact with particle B and starts heat diffusion. It can be observed that the shape of particle A has changed a little since it is in liquid phase. At 0.24 ms, particle A solidifies and sticks to particle B. From then on, they become a rigid body. At 0.32 ms and 0.44 ms, they keep moving towards right with some angular velocity.

Note that the X-ray image is 2D. Therefore, some overlapped particles can be observed. However, they may have different distance from the camera, which means that they may not contact even though they seem overlapping. The overlapping is severe at the powder bed, but the observation of particle A and B is not disturbed by the overlapping.

With the well-defined initial configuration which can retrieve the initial velocity of particle A, the SPH model can resemble the rest of the trajectories of both particles in the experiment. Thus, the matching result verities the validation of the SPH model, as well as its capability of simulating the sticking phenomenon in the L-PBF process.

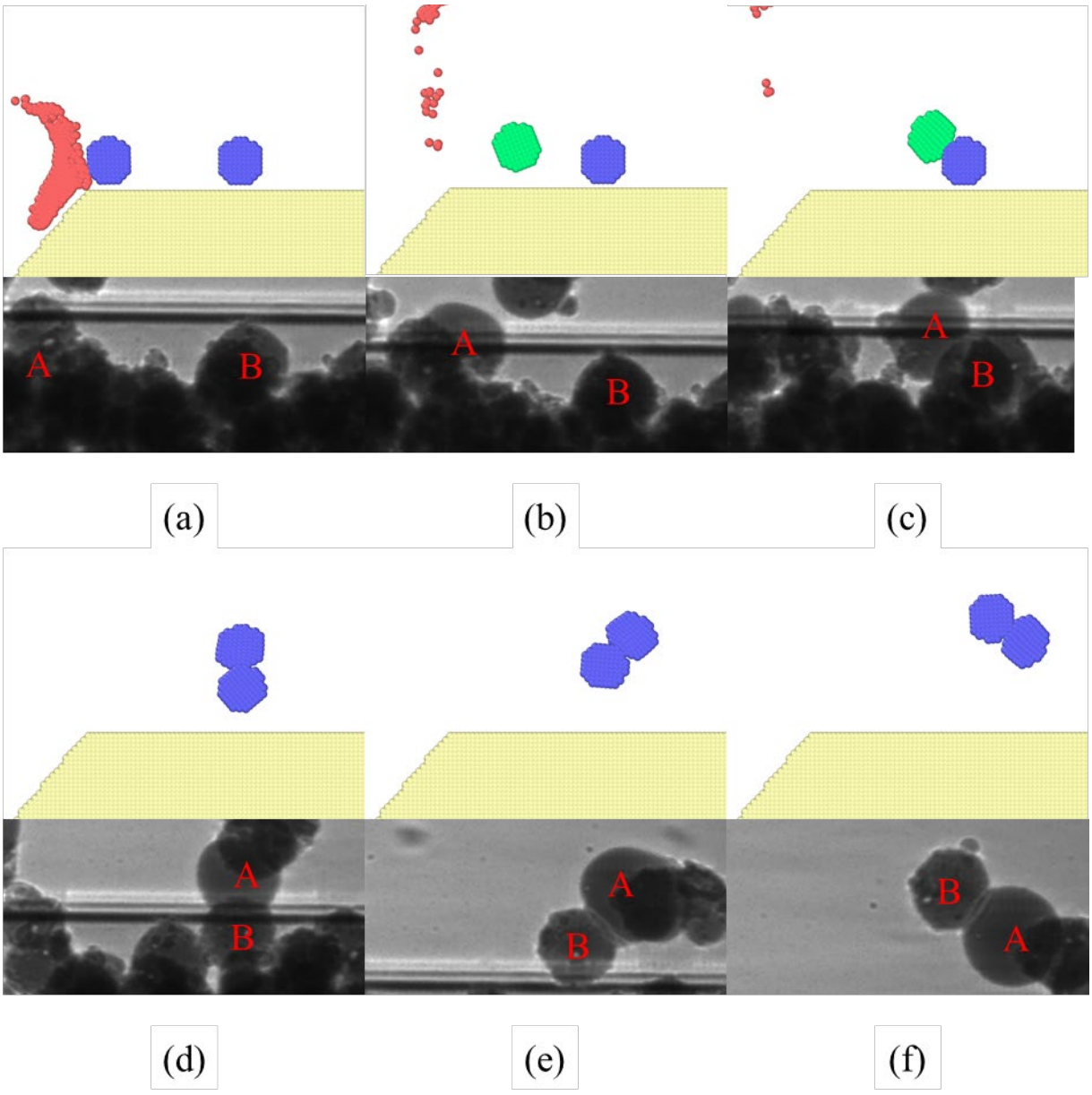

Figure 3. Trajectories of particle A and B in simulation (top) and experiment (bottom). Particle A in green color means it is melted. (a) 0 ms, (b) 0.08 ms, (c) 0.14 ms, (d) 0.24 ms, (e) 0.32 ms, (f) 0.44 ms

3.3. Velocity evolution

The velocity of particle A during the simulation is plotted in Figure 4, with the same time domain in Section 3.2. At 0.02 ms, the interaction between the vapor and the particle ends, and therefore the particle keeps a constant velocity for several microseconds. At 0.14 ms, particle A impact with particle B, and a significant change on the velocity of particle A can be observed.

From then on, particle A and particle B become a rigid body. Their motion is a combination of translation and rotation. As a result, the velocity of particle A in the rest of the simulation changes like a sine function.

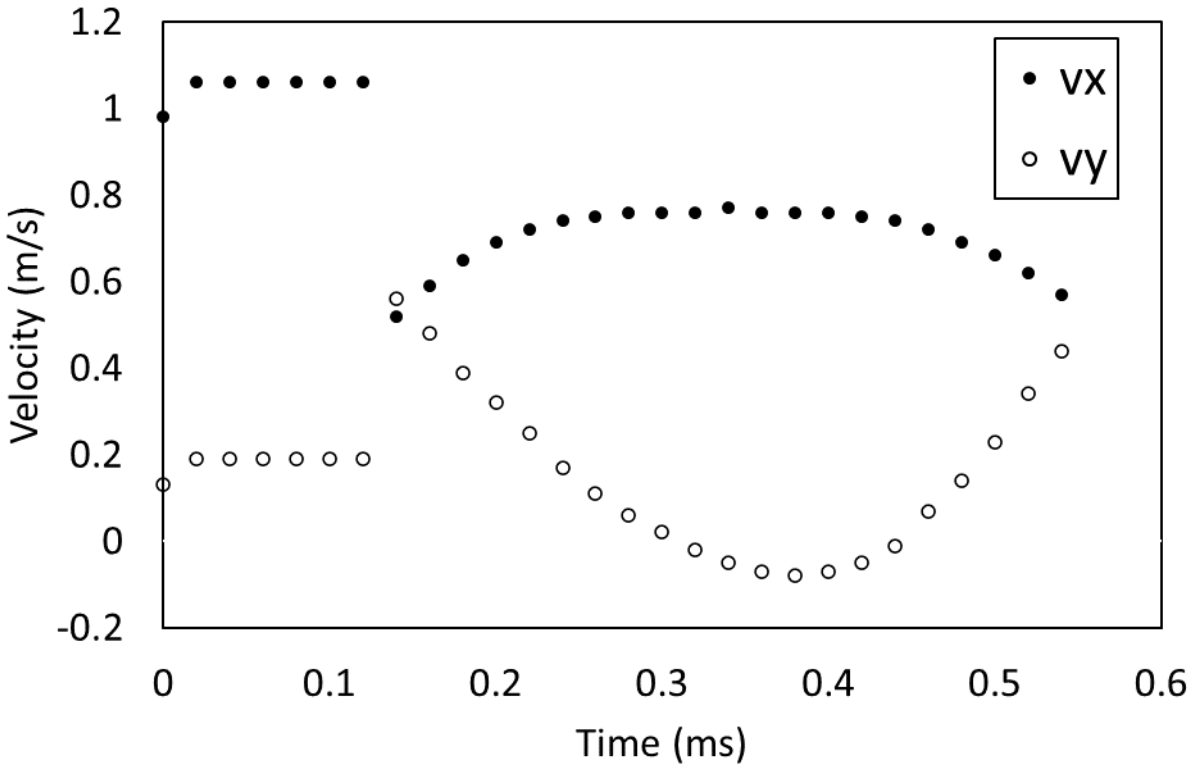

Figure 4. Evolution of velocity of particle A.

The effect of gravity cannot be observed in the simulation, as the magnitude of time is in microsecond. This phenomenon has also been explained by Guo *et al.* [32] using equivalent pressure. However, according to their quantification of angular powder velocity profile driven by metal vapor, the air resistance plays an important role in the deacceleration of the spatters. This phenomenon is not captured in this simulation as the effect of air is ignored.

3.4. Temperature evolution

Temperature evolution of the particles is difficult to be acquired from the experiment. Therefore, extracting temperature evolution is a desirable capability of computational models. Here, the average temperature of particle A is extracted from the simulation, shown in Figure 4.

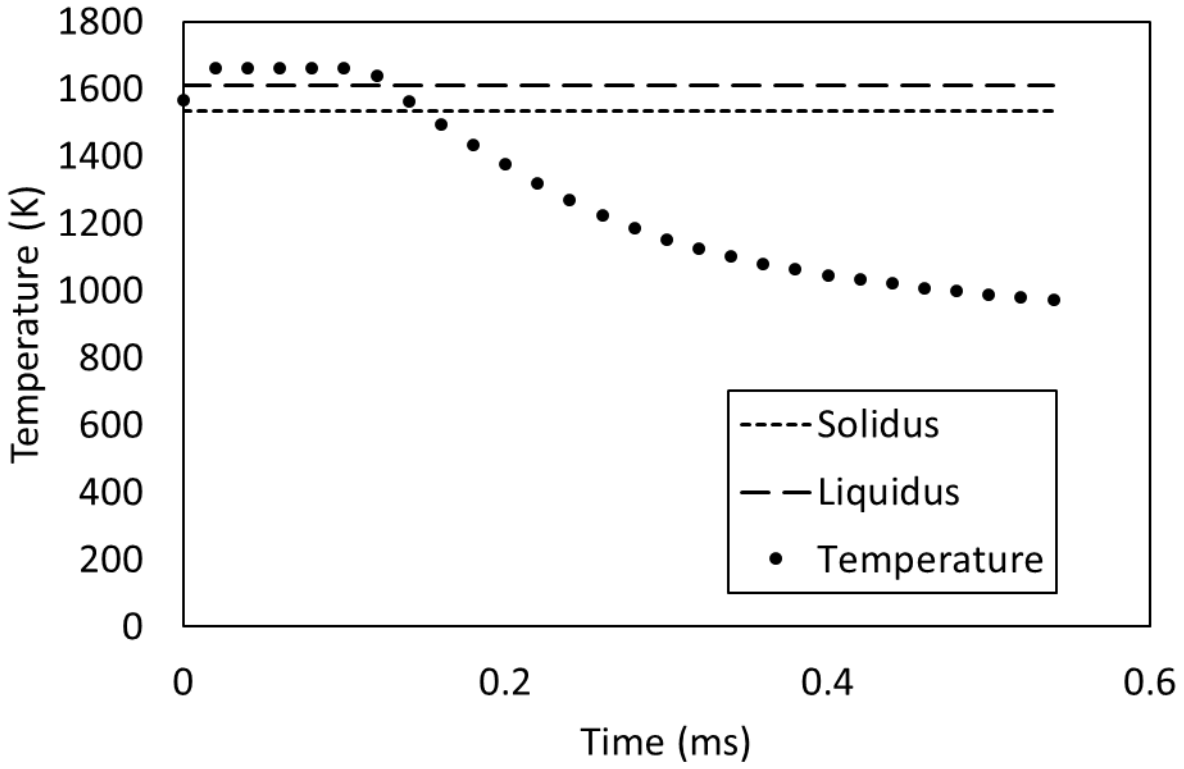

Figure 5. Evolution of the average temperature of particle A.

At 0 ms, the average temperature of particle A exceeds the solidus, but it does not reach the liquidus, and therefore the particle has not melted yet. After the interaction between metal vapor and particle A, the particle melts, and keeps a constant temperature as the air cooling is not captured in this simulation. Upon impacts with particle B, particle A cools down through heat diffusion, and therefore it solidifies right after the impact. After the solidification, particle A and B become a rigid body. In the rest of the simulation, the heat diffusion continues, with a decreasing cooling rate as the temperature difference between particle A and B decreases.

So far, the capability of simulating heat transfer, particle motion and phase change of the SPH model is demonstrated. The sticking phenomenon observed from the experiment is simulated. The trajectories of particles in the simulation match well with experiment. Though there are limitations in the model shown in this work, the SPH method can be an excellent alternate of the computational models used to simulate the spattering phenomenon.

4. Conclusions and Future Work

In this work, the SPH method is proposed to simulate the spattering phenomenon in the L-PBF process. A model is developed to perform a case study with the same scenario as the experiment. The major finding is summarized as follows:

1. The SPH model can resemble the trajectories of the particles and simulate the sticking phenomenon observed in the experiment. The simulation result matches well with experimental result.
2. The L-PBF process involves physical phenomena including heat transfer, phase change and particle motion, which is difficult to be simulated in one computational model like CFD. The paper demonstrates the capability of SPH in simulating these physical phenomena.
3. The phase change is done by the particle type change capability in LAMMPS when certain conditions (solidus and liquidus) are matched. In spite of the assumption of infinite rate of phase change, the SPH simulation package with adjustable rate of phase change may be included.

There are still some limitations in the model demonstrated in this work. These limitations include the missing effects of air resistance and air cooling, the difficulty in defining boundary conditions like fluid inlet and outlet, the assumed infinite rate of phase change, and the lack of the third dimension. Future work on improving the SPH model to overcome these limitations will be recommended.

Acknowledgement

The authors thank you Dr. Tao Sun at Argonne National Laboratory (now Associate Professor at University of Virginia) for providing the experimental data in Figure 3.

References

[1] G. Tapia and A. Elwany, "A Review on Process Monitoring and Control in Metal-Based Additive Manufacturing," *Journal of Manufacturing Science and Engineering,* vol. 136, no. 6, pp. 060801-060801-10, 2014.

[2] L. E. Criales *et al.*, "Laser powder bed fusion of nickel alloy 625: experimental investigations of effects of process parameters on melt pool size and shape with spatter analysis," vol. 121, pp. 22-36, 2017.

[3] M. Simonelli *et al.*, "A study on the laser spatter and the oxidation reactions during selective laser melting of 316L stainless steel, Al-Si10-Mg, and Ti-6Al-4V," vol. 46, no. 9, pp. 3842-3851, 2015.

[4] V. Gunenthiram *et al.*, "Experimental analysis of spatter generation and melt-pool behavior during the powder bed laser beam melting process," vol. 251, pp. 376-386, 2018.

[5] Y. Liu, Y. Yang, S. Mai, D. Wang, C. J. M. Song, and Design, "Investigation into spatter behavior during selective laser melting of AISI 316L stainless steel powder," vol. 87, pp. 797-806, 2015.

[6] C. Zhao *et al.*, "Real-time monitoring of laser powder bed fusion process using high-speed X-ray imaging and diffraction," vol. 7, no. 1, p. 3602, 2017.

[7] M. T. Andani, R. Dehghani, M. R. Karamooz-Ravari, R. Mirzaeifar, J. J. M. Ni, and Design, "Spatter formation in selective laser melting process using multi-laser technology," vol. 131, pp. 460-469, 2017.

[8] Q. Guo *et al.*, "Transient dynamics of powder spattering in laser powder bed fusion additive manufacturing process revealed by in-situ high-speed high-energy x-ray imaging," vol. 151, pp. 169-180, 2018.

[9] J. Yin *et al.*, "Correlation between forming quality and spatter dynamics in laser powder bed fusion," *Additive Manufacturing,* vol. 31, p. 100958, 2020.

[10] B. Cheng and A. H. J. C. M. S. Ngan, "The sintering and densification behaviour of many copper nanoparticles: A molecular dynamics study," vol. 74, pp. 1-11, 2013.

[11] Q. Mao, Y. Ren, K. H. Luo, and S. J. T. J. o. P. C. C. Li, "Sintering-induced phase transformation of nanoparticles: A molecular dynamics study," vol. 119, no. 51, pp. 28631-28639, 2015.

[12] J. Xu *et al.*, "Molecular dynamics simulation of Ni nanoparticles sintering process in Ni/YSZ multi-nanoparticle system," vol. 117, no. 19, pp. 9663-9672, 2013.

[13] F. Rahmani, J. Jeon, S. Jiang, and S. J. J. o. N. R. Nouranian, "Melting and solidification behavior of Cu/Al and Ti/Al bimetallic core/shell nanoparticles during additive manufacturing by molecular dynamics simulation," vol. 20, no. 5, p. 133, 2018.

[14] Y. Zhang and J. Zhang, "Sintering phenomena and mechanical strength of nickel based materials in direct metal laser sintering process—a molecular dynamics study," *Journal of Materials Research,* vol. 31, no. 15, pp. 2233-2243, 2016.

[15] Y. Zhang *et al.*, "Additive Manufacturing of Metallic Materials: A Review," *Journal of Materials Engineering and Performance,* journal article vol. 27, no. 1, pp. 1-13, 2018.

[16] S. A. Khairallah and A. J. J. o. M. P. T. Anderson, "Mesoscopic simulation model of selective laser melting of stainless steel powder," vol. 214, no. 11, pp. 2627-2636, 2014.

[17] S. A. Khairallah, A. T. Anderson, A. Rubenchik, and W. E. King, "Laser powder-bed fusion additive manufacturing: Physics of complex melt flow and formation mechanisms of pores, spatter, and denudation zones," *Acta Materialia,* vol. 108, pp. 36-45, 2016.

[18] S. Ly, A. M. Rubenchik, S. A. Khairallah, G. Guss, and M. J. J. S. r. Matthews, "Metal vapor micro-jet controls material redistribution in laser powder bed fusion additive manufacturing," vol. 7, no. 1, p. 4085, 2017.
[19] M. J. Matthews, G. Guss, S. A. Khairallah, A. M. Rubenchik, P. J. Depond, and W. E. J. A. M. King, "Denudation of metal powder layers in laser powder bed fusion processes," vol. 114, pp. 33-42, 2016.
[20] P. Bidare, I. Bitharas, R. Ward, M. Attallah, and A. J. A. M. Moore, "Fluid and particle dynamics in laser powder bed fusion," vol. 142, pp. 107-120, 2018.
[21] R. A. Gingold and J. J. Monaghan, "Smoothed particle hydrodynamics: theory and application to non-spherical stars," *Monthly notices of the royal astronomical society,* vol. 181, no. 3, pp. 375-389, 1977.
[22] L. B. Lucy, "A numerical approach to the testing of the fission hypothesis," *The astronomical journal,* vol. 82, pp. 1013-1024, 1977.
[23] L. D. Libersky and A. G. Petschek, "Smooth particle hydrodynamics with strength of materials," in *Advances in the free-Lagrange method including contributions on adaptive gridding and the smooth particle hydrodynamics method*: Springer, 1991, pp. 248-257.
[24] F. A. Allahdadi, T. C. Carney, J. R. Hipp, L. D. Libersky, and A. G. Petschek, "High strain lagrangian hydrodynamics: a three dimensional SPH code for dynamic material response," Phillips Lab Kirtland AFB NM1993.
[25] G. C. Ganzenmüller and M. O. Steinhauser. (2011, May 4th). *The implementation of Smooth Particle Hydrodynamics in LAMMPS*. Available: https://lammps.sandia.gov/doc/PDF/SPH_LAMMPS_userguide.pdf
[26] G. C. Ganzenmüller. (2014, May 4th). *Smooth Mach Dynamics*. Available: https://lammps.sandia.gov/doc/PDF/SMD_LAMMPS_userguide.pdf
[27] G.-R. Liu and M. B. Liu, *Smoothed particle hydrodynamics: a meshfree particle method*. World scientific, 2003.
[28] S. Plimpton, "Fast parallel algorithms for short-range molecular dynamics," Sandia National Labs., Albuquerque, NM (United States)1993.
[29] N. D. Parab *et al.*, "Ultrafast X-ray imaging of laser–metal additive manufacturing processes," *Journal of synchrotron radiation,* vol. 25, no. 5, 2018.
[30] A. Stukowski, "Visualization and analysis of atomistic simulation data with OVITO–the Open Visualization Tool," *Modelling and Simulation in Materials Science and Engineering,* vol. 18, no. 1, p. 015012, 2009.
[31] G. Pottlacher, H. Hosaeus, E. Kaschnitz, and A. Seifter, "Thermophysical properties of solid and liquidInconel 718 Alloy," *Scandinavian Journal of Metallurgy,* vol. 31, no. 3, pp. 161-168, 2002.
[32] Q. Guo *et al.*, "Transient dynamics of powder spattering in laser powder bed fusion additive manufacturing process revealed by in-situ high-speed high-energy x-ray imaging," *Acta Materialia,* vol. 151, pp. 169-180, 2018.